High-order LES of turbulent heat transfer in a rotor–stator cavity

Sébastien Poncet, Eric Serre

High-order LES of turbulent heat transfer in a rotor-stator cavity

Sébastien Poncet* and Éric Serre†

MSNM-GP, UMR 6181 CNRS- Universités d'Aix-Marseille

IMT La Jetée, Technopôle Château-Gombert, 38 rue F. Joliot-Curie,

13451 Marseille cédex 20 - FRANCE - Fax. 0033.(0)4.91.11.85.02

(Dated: January 16, 2009)

The present work examines the turbulent flow in an enclosed rotor-stator system subjected to heat transfer effects. Besides their fundamental importance as three-dimensional prototype flows, such flows arise in many industrial applications but also in many geophysical and astrophysical settings. Large eddy simulations (LES) are here performed using a Spectral Vanishing Viscosity technique. The LES results have already been favorably compared to velocity measurements in the isothermal case [23] for a large range of Reynolds numbers $10^5 \leq Re = \Omega b^2/\nu \leq 10^6$, in an annular cavity of large aspect ratio $G = (b-a)/H = 5$ and weak curvature parameter $R_m = (b-a)/(b+a) = 1.8$ (a, b the inner and outer radii of the rotor and H the interdisk spacing). The purpose of this paper is to extend these previous results in the non-isothermal case using the Boussinesq approximation to take into account the buoyancy effects. Thus, the effects of thermal convection have been examined for a turbulent flow $Re = 10^6$ of air in the same rotor-stator system for Rayleigh numbers up to $Ra = 10^8$. These LES results provide accurate, instantaneous quantities which are of interest in understanding the physics of turbulent flows and heat transfers in an interdisk cavity. Even at high Rayleigh numbers, the structure of the iso-values of the instantaneous normal temperature gradient at the disk surfaces resembles the one of the iso-values of the tangential velocity with large spiral arms along the rotor and more thin structures along the stator. The averaged results show small effects of density variation on the mean and turbulent fields. The turbulent Prandtl number is a decreasing function of the distance to the wall with 1.4 close to the disks and about 0.3 in the outer layers. The local Nusselt number is found to be proportional to the local Reynolds number to the power 0.7. The evolution of the averaged Bolgiano length scale $< L_B >$ with the Rayleigh number indicates that

temperature fluctuations may have a large influence on the dynamics only at the largest scales of the system for $Ra \geq 10^7$, since $< L_B >$ remains lower than the thermal boundary layer thicknesses.

Keywords: Large Eddy Simulation, rotor-stator, heat transfer, Boussinesq approximation.

*Electronic address: poncet@l3m.univ-mrs.fr,Tel.0033.(0)4.91.11.85.23

†Electronic address: serre1@l3m.univ-mrs.fr,Tel.0033.(0)4.91.11.85.35

I. INTRODUCTION

The effects of convective heat transfers on the turbulent air flow in an enclosed rotor-stator cavity are here investigated by large eddy simulation (LES) using the Boussinesq approximation. The interdisk spacing is sufficiently large to ensure that the boundary layers developed on each disk are separated. Thus, the present study is focused on flows belonging to the regime IV (turbulent Batchelor flows with separated boundary layers) of Daily and Nece [7]. The cavity is heated from below along the stator side, while the upper disk is rotating and cooled. Thus, it is an unstable configuration, where the density gradient is opposed to gravity acceleration.

These flows are important in a large number of industrial applications such as in disk drives used for digital data storages in computers, in the ventilation of electrical air cycle machines, in semi conductor manufacturing processes with rotating wafers and in a lot of other rotating machineries like generator rotors or gas turbine engines. For example, in high-speed rotating gas turbines, the cooling air flow is used to both cooling the disk and preventing the ingestion of hot turbine passage gases into the cavity. A good knowledge of heat transfers and fluid flows in such systems is crucial: an excessive amount of coolant is often supplied to the cavity that imposes an unnecessary penalty on the engine cycle and leads to a loss of efficiency.

At that time, most of the published works have dealt with the isothermal fluid flow aspects in a rotor-stator system [7, 23] mainly because of the complexity and the cost of making accurate heat transfer measurements. A large review of the fundamental investigations relevant to heat and mass transfers in rotor-stator cavities carried out until 1989 has been performed by Owen and Rogers [17]. In the regime IV [7], the dynamics of thermal convection with a rotating top wall can be characterized essentially by three global physical parameters in a closed cavity, which are the rotational Reynolds number Re, the Rayleigh number Ra and the Prandtl number Pr defined by:

$$Re = \Omega b^2/\nu \qquad Ra = \frac{\Omega^2 b \Delta T H^3}{\nu \kappa T_r} \qquad Pr = \frac{\nu}{\kappa}$$

where ν and κ are the kinematic viscosity and the thermal diffusivity of the fluid, respectively. Ω is the rotation rate of the disk, b the disk radius, H the interdisk spacing, ΔT the temperature difference between the disks and T_r is the temperature of reference equal to the

mean of the wall temperatures. The total heat flux through the disks is usually expressed in terms of the local Nusselt number $Nu = hr/\lambda$ (h the convective heat transfer coefficient, r the local radius and λ the conductivity of the fluid) or of the averaged Nusselt number Nu_{av}. Note that h, the convective heat transfer coefficient, is obtained by dividing the local rate of wall heat transfer calculated from the nodal values of temperature, by ΔT the difference between the stator and rotor uniform temperatures. Both depend in a complicated manner on (Ra, Re, Pr) but also on the flow rate coefficient for open cavities. The influence of the aspect ratio $G = b/H$ of the cavity on the distribution of the local Nusselt number along the disks is weak compared to the ones of rotation for example [17].

In the regime IV, Dorfman [10] proposes, from experiments, a correlation for the local Nusselt number on the rotor for rotor-stator flows above isothermal disks:

$$Nu = 0.0197 Pr^{0.6} Re_r^{0.8} \tag{1}$$

with Re_r the local Reynolds number based on the radial location r. Note that the aspect ratio and the Rayleigh number do not appear in this correlation. Dorfman [10] proposes other correlations depending on the temperature distributions imposed on the disks. This author showed also that heat transfer on the rotating disk was not affected by the presence of the stator for $H/b \geq 1.05 Re^{-0.2}$, which is the case in the present study. That implies that the correlation laws obtained in the single disk case [10, 17] can also be applicable here. Daily and Nece [7] proposed a correlation for the mean Nusselt number on the rotor:

$$Nu_{av} = 0.0173 (\frac{1}{2G})^{0.1} Re^{0.8} \tag{2}$$

Relatively few experimental data are available in the literature for heat transfer in rotating disk flows. Djaoui et *al.* [8, 9] examined the turbulent flow in a rotor-stator cavity of large aspect ratio subjected to a superimposed radial inflow and heat transfer effects. Detailed velocity and Reynolds stress tensor measurements as well as temperature and temperature-velocity correlations have been carried out using a hot and cold wire anemometry technique. The temperature distribution was specified on the stator and heat transfer coefficient controlled with the help of pellicular fluxmeters. They studied in particular the external peripheral geometry effects and the critical importance of the inlet conditions on the mean tangential fluid velocity. They focused also on the dependence of the flow structure and heat

transfer effects on the Rossby and Reynolds numbers. Comparisons with an asymptotical formulation based on the assumption of inviscid fluid were displayed and were shown to be in good agreement with the experimental data. Elkins and Eaton [11] performed detailed measurements of mean velocities and temperatures as well as measurements of all six Reynolds stress tensor components, turbulent temperature fluctuations and three turbulent heat fluxes in the case of a rotating single disk with an uniform heat flux surface. They showed that for turbulent flows up to $Re = 10^6$ and temperature differences up to $\Delta T = 10.8$ K, temperature may be considered as a passive scalar. The disk thermal boundary layer exhibits some characteristics of three-dimensional turbulent boundary layer. Harmand et *al.* [13] investigated both the flow structure by Particule Image Velocimetry (PIV) and the heat transfers using a thermally rotor heated by infrared radiation in the case of turbulent rotor-stator flows. The local heat flux distribution from the rotor was identified by solving the Laplace equation by finite difference. The local Nusselt number Nu on the rotor was found to be an increasing function of the Reynolds number and remains almost constant along the radius contrary to the free disk case, where Nu increases from the axis to the periphery of the cavity. Pellé and Harmand [18] studied experimentally the influence of the dimensionless interdisk spacing G on the local Nusselt number. It remained almost constant whatever the Reynolds number for $G = 12.5$. They identified four heat transfer regimes corresponding to the four flow regimes of Daily and Nece [7] and gave correlations for the local and averaged Nusselt numbers depending on the aspect ratio and the Reynolds number. For turbulent flows with separated boundary layers, the general laws for Nu and Nu_{av} are:

$$Nu = 0.035(1 - e^{-40/G})(1 - e^{-4.2\times10^5 Re})Re_r^{0.746} \tag{3}$$

$$Nu_{av} = 0.0325(1 - e^{-40/G})(1 - e^{-4.2\times10^5 Re})Re^{0.746} \tag{4}$$

The fact that only few experimental works have been done has slowed down the development of advanced heat transfer models. Abe et *al.* [1] developped a two-equation heat transfer model, which incorporates essential features of second-order modeling. They introduced the Kolmogorov velocity scale to take into account the low Reynolds number effects in the near-wall region and also complex heat transfer fields with flow separation and reattachement. But this model has not been yet implemented for rotating disk flows. A major

numerical work is the one of Iacovides and Chew [14]. They have used four different models of turbulence to study the convective heat transfer in three axisymmetric rotating disk cavities with throughflow. Three models were based on a zonal modeling approach and one was based on a mixing-length hypothesis. Their numerical predictions were compared to experimental data available in the literature but none of the four models was entirely successful. Nevertheless, considering overall performance, the $k-\epsilon$ model with the one-equation near-wall treatment was preferred. Schiestel et *al.* [21] have examined the turbulent flow in a rotating cavity with a radial outward throughflow and heat transfer effects. They compared a standard $k-\epsilon$ low-Reynolds number model and a zonal approach using second-order Algebraic Stress Model (ASM) in the core of the flow. They showed that second-order modeling is necessary to obtain a detailed near-wall treatment. Roy et *al.* [20] performed numerical simulations using the CFD code Fluent to provide an empirical correlation for Nu along the rotor:

$$Nu = 0.0074 Re_r^{0.89} \tag{5}$$

Recently, Poncet and Schiestel [19] compared a second order moment closure (Reynolds Stress Model) sensitized to rotation effects to data available in the literature. They considered the temperature as a passive scalar ($Ra = 0$) and found a close agreement in the case of an open cavity even for large temperature differences. They provided an empirical correlation for the problem considered by Djaoui et *al.* [8, 9], which can be extended in the case of a closed cavity to:

$$Nu_{av} = 0.0094 Re^{0.8} Pr^{0.5} \tag{6}$$

Finally, all workers concluded that further experimental but also numerical research is required before a mathematical model can be recommanded with any confidence.

As already mentioned, the difficulty and the cost of measurements under severe conditions of rotation and temperature do not allow a full description of the mean and turbulent fields. As a consequence, numerical modeling became a valuable tool for predicting flow structure and heat transfer effects in industrial configurations. Previous works [19] have shown that second-order modeling is a good way to predict the flow structure in a high-speed rotor-stator cavity with throughflow and heat transfers for Re up to 4×10^6 and $\Delta T = 75$ K. Neverthe-

less, turbulence modeling does not take into account three-dimensional effects due to highly structured large-scale vortices, which have a large influence on the resultant heat transfer coefficients at the disk surface. Bohn et *al.* [2] have indeed shown both experimentally and numerically that co- and contra-rotating vortices induced by the gravitational buoyancy force can appear in a rotating cavity with an axial throughflow of cooling air. These pair of vortices are very similar to the ones observed by Czarny et *al.* [5] in a rotor-stator cavity under isothermal conditions. Thus, accurate three-dimensional numerical simulations are required to investigate non-isothermal rotating disk flows. Serre et *al.* [22] performed direct numerical simulations (DNS) of non-isothermal transitional flows under the Boussinesq approximation at a moderate Reynolds number $Re = 1.1 \times 10^5$. They showed in particular that the effects of density variation remain small for Rayleigh numbers up to $Ra = 2 \times 10^6$.

The purpose of the present work is to propose, for the first time, three-dimensional accurate calculations of turbulent rotor-stator flows under non-isothermal conditions in an actual enclosed cavity. The objective is then to acquire precise knowledge of both the flow structure and the temperature distribution on the disks in order to predict durability and determine the disk dimensions for turbomachinery applications but also to assess the influence of rotation on convective flow for geophysical and astrophysical settings. The paper is organized as follows: we first describe the geometrical configuration and the numerical modeling. Then, flow structures are presented at a given Rayleigh number $Ra = 10^7$. The influence of the Rayleigh number on the mean and turbulent fields is discussed afterwards to show the effects of density variation on the averaged results. Finally some conclusions and closing remarks are provided.

II. THE NUMERICAL MODELING

A spectral vanishing viscosity (SVV) method for LES has been recently developed for simulating rotating disk flows [24] and validated in the case of turbulent rotor-stator flows under isothermal conditions [23]. This approach has the property of preserving the spectral accuracy of the approximation developed in DNS and of keeping the fast time integration of the DNS because it is placed in pre-processing. The reader is referred to the work of Séverac and Serre [24] for more details about the numerical modeling.

A. Geometrical configuration

The cavity sketched in Figure 1 is composed of two smooth disks enclosed by an inner rotating cylinder (the hub) and an outer stationary casing (the shroud). The lower disk is stationary (the stator) and heated, while the upper disk is rotating and cooled. The rotor and the central hub attached to it rotate at the same uniform angular velocity Ω. The hydrodynamic flow is governed by three main control parameters: the aspect ratio of the cavity G, the curvature parameter R_m and the rotational Reynolds number Re based on the outer radius b of the rotating disk defined as follows:

$$G = \frac{b-a}{H} = 5 \qquad R_m = \frac{b+a}{b-a} = 1.8 \qquad Re = \frac{\Omega b^2}{\nu} = 10^6$$

where ν is the kinematic viscosity of water, $a = 40$ mm and $b = 140$ mm the inner and outer radii of the rotating disk and $H = 20$ mm the interdisk spacing. We define also the radial $r^* = (r-a)/(b-a)$ and axial $z^* = z/H$ coordinates. Thus $r^* = 0$ is obtained on the hub and $r^* = 1$ on the shroud. In the same way, $z^* = 0$ on the stator disk and $z^* = 1$ on the rotor disk. The values of the geometrical parameters G and R_m have been chosen in order to be relevant with industrial devices such as a real stage of turbopump, and to satisfy technical constraints of the experimental device in the isothermal case as well as computational effort to reach statistically converged stages [23]. The value of Re is also fixed to the highest value reached in the hydrodynamical case $Re = 10^6$ [23] in order to highlight only the thermal effects.

Conducting and insulating thermal boundary conditions have been considered on the disks and the cylinders, respectively. The temperature is normalized by the temperature difference applied between the stator and the rotor: $T^* = 2(T - T_r)/\Delta T$ with $\Delta T = T_{hot} - T_{cold}$ and $T_r = (T_{hot} + T_{cold})/2$. The stator is thus maintained at the constant dimensionless temperature $T^* = 1$, while the rotor is maintained at the constant dimensionless temperature $T^* = -1$. The hub and the shroud are thermally insulated with zero heat flux. The Prandtl number Pr and the Rayleigh number Ra based on the maximum radial acceleration have also to be taken into account to study the flow dynamics. They are defined as follows:

$$Pr = \frac{\nu}{\kappa} = 0.7 \qquad 0 \leq Ra = \frac{\Omega^2 b \Delta T H^3}{\nu \kappa T_r} \leq 10^8$$

where κ is the thermal diffusivity of the fluid. Note that the value of Pr chosen here corresponds to the typical value for air at 293 K. For this value of Prandtl number, the

thermal diffusivity is slightly dominant. In a classical Rayleigh-Bénard system without rotation, there is no motion for $Pr = 0.7$ until the appearance of steady rolls at $Ra = 5 \times 10^3$ [12]. All the parameters are then fixed except for the Rayleigh number Ra, whose influence on the flow dynamics is here investigated. To have an idea of the physical temperature difference between the disks, if the temperature of the rotor is fixed to the initial temperature of air $T_{cold} = 293$ K, the maximum value of the Rayleigh number $Ra = 10^8$ corresponds to a temperature difference of 15.82 K, which is 50% larger than the temperature difference considered by Elkins and Eaton [11]. Thus, some thermal effects may be expected in the present case.

B. Governing equations

The motion is governed by the incompressible three-dimensional Navier-Stokes equations written below in cylindrical polar coordinates (r,θ,z) using a velocity-pressure formulation, together with the continuity equation and appropriate boundary conditions. The velocity-temperature coupling is dealt using the Boussinesq approximation. Then, we have:

$$\nabla \mathbf{V} = 0 \tag{7}$$

$$\frac{\partial \mathbf{V}}{\partial t} + \mathbf{V}.\nabla \mathbf{V} = -\nabla P^* + \frac{1}{Re}\nabla^2 \mathbf{V} + Ra\, T^*\, \mathbf{e_z} \tag{8}$$

$$\frac{\partial T^*}{\partial t} + \mathbf{V}.\nabla T^* = \frac{1}{Pr}\nabla^2 T^* \tag{9}$$

where $\mathbf{V} = (V_r^*, V_\theta^*, V_z^*)$ is the velocity vector, P^* the pressure and T^* the temperature. The velocity, space and time scalings correspond to Ωb, h and Ω^{-1} respectively.

C. Numerical method

The pseudospectral numerical method is based on a collocation-Chebyshev method in the radial r and axial z non-homogeneous directions and a Galerkin-Fourier method in the azimuthal periodic direction θ. Thus, each dependent variable $f = (V_r, V_\theta, V_z, P)$ is expanded into a truncated trigonometric series on T_n and T_m, a Chebyshev polynomial basis of degrees n and m respectively. This approximation is applied at the Gauss-Lobatto collocation points, where the differential equations are assumed to be satisfied exactly, defined as $r_i = cos(\frac{i\pi}{N})$

for $i \in [0, N]$ and $z_j = cos(\frac{j\pi}{M})$ for $j \in [0, M]$ in the radial and axial directions. In the azimuthal direction, an uniform distribution is considered: $\theta_k = 2k\pi/K$ for $k \in [0, K[$. N, M define the number of collocation points in the radial and axial directions respectively and K is the cutoff in the tangential direction. In the meridional plane, the space variables $(r, z) \in [a, b] \times [0, h]$ have been normalized into the square $[-1, 1] \times [-1, 1]$, a prerequisite for the use of Chebyshev polynomials.

The time scheme is semi-implicit and second order accurate. It is a combination of an explicit treatment of the convective terms (Adams-Bashforth scheme) and of an implicit treatment for the diffusive terms (second order backward Euler scheme). The solution method is based on an efficient projection scheme to solve the coupling between velocity and pressure. This algorithm ensures a divergence-free velocity field at each time step, maintains the order of accuracy of the time scheme for each dependent variable and does not require the use of staggered grids. Finally, for each Fourier mode, a full diagonalization technique is used and yields simple matrix products for the solution of successive two-dimensional uncoupled Helmholtz and Poisson equations at each time step.

The Spectral Vanishing Viscosity (SVV) is incorporated into the cylindrical Navier-Stokes equations. A viscosity kernel operator, only active for high wave numbers of the numerical approximation, is incorporated in the Helmholtz equations of velocity prediction [24]. Then, the diffusion and SVV terms are combined in order to obtain a new diffusion operator that can be easily written in 1D:

$$\nu\Delta_{SVV}v_N = \nu\Delta v_N + \varepsilon_N\partial x(Q_N.\frac{\partial v_N}{\partial x}) \tag{10}$$

where v_N is the velocity vector approximation and Q_N is the kernel defined in the spectral space as:

$$\hat{Q_N}(w_n) = \begin{cases} 0 & \text{for } 0 \leq w_n \leq w_T \\ \epsilon_N.e^{-(\frac{w_N - w_n}{w_T - w_n})^2} & \text{for } w_T < w_n \leq w_N \end{cases} \tag{11}$$

with ϵ_N the maximum of viscosity, w_T the mode after which the spectral viscosity is applied and w_N the highest mode calculated. Thus, the viscosity kernel is zero on the lower frequencies. There is no direct way to extend the one dimensional definition of the SVV operator to the three-dimensional case. Then, Séverac and Serre [24] proposed the following definition which has been used here:

$$\nu\Delta_{SVV}v_N = \nu\Delta v_N + \nabla.(\varepsilon_N Q_N(\nabla v_N)) \tag{12}$$

where ∇v_N is the Jacobian of the vectorial function v_N, $\varepsilon_N Q_N \equiv \varepsilon^i_{Ni} Q^i_{Ni}$ with $i = 1, 2, 3$ (corresponding to the r, θ, z directions respectively), and where ε^i_{Ni}, Q^i_{Ni} are the maximum of viscosity and the 1D viscosity operator acting in direction i, respectively.

D. Computational details

The initial condition corresponds to a fluid at rest. No-slip boundary conditions are applied to all walls. There, $V_r = V_z = 0$ on all walls, whereas V_θ is fixed at zero on the stator and the shroud and at the local disk velocity Ωr on the rotor and the hub. At the junctions rotor-stator, the tangential velocity component has been regularized using a boundary function $V^*_\theta = e^{(z^*-1)/\mu}$, with $\mu = 0.006$ an arbitrary shape parameter independent of the grid size. This function provides a reasonable representation of experimental conditions [23], while retaining spectral accuracy. The boundary conditions imposed on the four walls are summed up below:

$$\begin{cases} V_r = 0,\ V_\theta = \Omega r,\ V_z = 0,\ T = T_{cold}, & \text{rotor} \\ V_r = 0,\ V_\theta = 0,\ \ V_z = 0,\ T = T_{hot}, & \text{stator} \\ V_r = 0,\ V_\theta = \Omega a,\ V_z = 0,\ \partial T/\partial r = 0, & \text{hub } (r = a) \\ V_r = 0,\ V_\theta = 0,\ \ V_z = 0,\ \partial T/\partial r = 0, & \text{shroud } (r = b) \end{cases} \tag{13}$$

As shown previously, the SVV operator is parametrized in each direction by (w_T, ϵ_N). According to previous results obtained by Séverac and Serre [24], good values of such parameters are $w_T \approx O(\sqrt{N})$ and $\epsilon_N \approx O(1/N)$, where N is the degree of approximation in each direction. These values have also provided a good compromise between stability and accuracy in former numerical studies. Let's notice that SVV operator affects at most the two-third of the spectrum on the highest frequencies ($w_T = 0$) and consequently, DNS results are easily recovered for laminar flows, contrarily to some classical LES techniques. The SVV parameters have been chosen in order to stabilize the calculation while dissipating artificially the least possible: ϵ_N=$1/N$ in the three directions and w_T=$2\sqrt{N}, 5\sqrt{N}, 4\sqrt{N}$ in the (r,θ,z) directions respectively.

A $(151, 241, 81)$ grid in the (r,θ,z) directions respectively (about 2.95 millions of mesh

points) is sufficient to get grid independent solutions. It corresponds to a wall normal coordinate, which remains below or around 1 along the radius. Thus, the viscous sublayer is described by at least five collocation points. The computational domain has been restricted to ($[0, \pi]$) in order to save time. This hypothesis only allows even azimuthal modes of boundary layer instability, that does not change nor qualitatively nor quantitatively the features of turbulent flow as a wide range of modes are known to be unstable [23]. Moreover, all the previous investigations in isothermal configuration have shown the tendency of the flow structures to become axisymmetric when increasing the Reynolds number. Finally, some recent experiments (not published yet) have revealed that the three-dimensional structures, which subsist at very high Reynolds numbers in the core of a cylindrical rotor-stator cavity [4, 5], do not persist in the case of an annular cavity. Thus, there is no experimental or numerical evidence that three-dimensional well organized structures could appear in the present configuration.

The time step used in the present study is fixed to 10^{-5}. All the data have been averaged both in time and in the tangential direction. In the isothermal case, the average is performed on 464 disk revolutions. Then, this solution is used as an initial solution for the non-isothermal calculations. The data in the non-isothermal cases are averaged on 77 disk revolutions, which is sufficient as the averaging for the Nusselt number converges quite rapidly, about 20 dimensionless time units in the similar system of Kunnen et *al.* [16].

Note that the LES results have been already favorably compared in the isothermal case to velocity measurements performed at IRPHE using a two-component laser Doppler velocimeter (see in Séverac et *al.* [23]).

III. FLOW STRUCTURES

The flow is here analysed at $Ra = 10^7$ in the case of a turbulent flow ($Re = 10^6$) of air ($Pr = 0.7$). Instantaneous fields are first presented before quantifying the effect of Ra on the statistical data in the following section.

Figure 2 shows the iso-values of the instantaneous tangential velocity component $V_\theta/(\Omega b)$ in both boundary layers and the corresponding instantaneous normal temperature gradient $\partial T^*/\partial z^*$ at the disk surfaces, which is proportional to the local heat transfer rate through the surface. Although the grey scales do not correspond perfectly, it is clear that these heat-fluxes

pictures reveal the same structures as seen in the views of instantaneous velocity direction. Along the cooled rotor (Fig.2a), the structure of the iso-values of $\partial T^*/\partial z^*$ resembles the one of the iso-values of $V_\theta/(\Omega b)$ (Fig.2c) with large positive spiral arms (as they roll up in the sense of rotation of the disk) appearing at intermediate radial positions. They are enclosed by two turbulent flow regions (see in [23]). The first one is located at the junction between the rotor and the hub. The hot fluid coming from the stator side flows along the hub and impinges the rotor. It is then cooled by this disk. That is the reason why this turbulent flow region is characterized by a temperature equal to zero (see Fig.3a). The second region of high turbulence intensities appears at the periphery of the cavity where the highest values of the local Reynolds number prevail. The spiral arms disappeared and more thin structures are created. They are also characterized by a dimensionless temperature close to zero (see Fig.3a). The cooled fluid coming from the rotor after impingement on the shroud and then on the stator is heated by this lower disk. It creates a crown of fluid with a zero dimensionless temperature at the periphery of the cavity (see Fig.3a). Afterwards, this fluid flows along the stator from the periphery to the axis of the cavity. The fluid is progressively heated until the axis and so higher temperature levels are obtained (Fig.3a). The heat-fluxes picture is more chaotic in this boundary layer. It resembles to the one of the iso-values of $V_\theta/(\Omega b)$ with very thin structures (Fig.2d). To conclude, the pattern of heat transfer rate is strongly affected by any organized structure in the flow pattern.

Figure 3a presents the isotherms at $Ra = 10^7$ in a (r, z) plane. This map confirms that the fluid heated along the stator is carried along the hub (dark areas on Fig.3a) with a positive axial velocity ($V_z/(\Omega b) > 0$ corresponds to dark areas on Fig.3b) and then cooled by the fluid flowing along the rotor (bright areas on Fig.3a). In the same way, the flow cooled by the rotor impinges the shroud and then the stator to be heating along this wall. The axial velocity of the fluid in the Stewartson layer along the external cylinder is then negative (bright areas on Fig.3b). As a consequence, there are two regions along the walls of quasi zero temperature: at the junction between the hub and the rotor and at the junction between the shroud and the stator. The temperature in the core is also quasi equal to zero in the whole cavity, which means that the secondary flow in the wall layers is responsible for most of the heat transfer in the cavity. Nevertheless, it can be seen in Figure 3a that vertical thermal plumes appear along the stator, essentially for inner radii. They are characterized by a dimensionless temperature close to unity. The well defined vertical structure of these

plumes corresponds to regions of relatively high positive axial velocities (Fig.3b). At the periphery of the cavity, where the highest turbulence intensities are obtained, there are no thermal plumes due to the intense mixing between hot and cold fluids. Along the rotating disk, some cooled fluid is moving down with a smaller vertical extension (Fig.3a). Thus, the effect of the heated disk seems to dominate the heat transfer in the cavity.

IV. MEAN FLOW AND TURBULENCE STATISTICS

The aim of this section is to quantify the effect of the Rayleigh number Ra on the mean and turbulent flow fields, on the temperature field and then, on the heat fluxes along the disks for a turbulent air flow ($Pr = 0.7$, $Re = 10^6$). We recall that all the data have been averaged both in time and in the tangential direction. The mean velocity components and the normal components of the Reynolds stress tensor are respectively normalized as follows: $V_i^* = \overline{V_i}/(\Omega r)$ and $R_{ij}^* = \overline{v_i' v_j'}/(\Omega r)^2$ for $i, j = (r, \theta, z)$.

A. Flow field

To quantify the buoyancy effects on the flow field, we firstly define a convective Rossby number $Ro_c = \sqrt{Ra/(PrTa)}$, where $Ta = (2\Omega H^2/\nu)^2$ is the Taylor number equal to 1.67×10^9 in the present case. It compares the buoyancy forces and the Coriolis forces. For $Ro_c > 1$, buoyancy forces are larger than Coriolis forces.

Figure 4 shows axial profiles of the mean velocity components at four radial locations in the range $0.3 \leq r^* \leq 0.9$. Four values of the Rayleigh number have been considered and the results are compared to the isothermal case described in [23]. Whatever the value of Ra considered, the Batchelor flow model best describes the flow structure with fluid pumped radially outwards in the rotor boundary layer ($V_r^* > 0$ close to $z^* = 1$), called the Ekman layer, moving axially across the stator in the Stewartson boundary layer over the cylindrical outer shroud. Then, the fluid flows radially inward along the stator side ($V_r^* < 0$ close to $z^* = 0$), in the Bödewadt layer, and impinges the rotating inner hub before going along the rotor again. The rotor and stator boundary layers are separated by an inviscid rotating core of fluid that rotates at around 38% of the rotating disk velocity, value which slightly depends on the radial location [23]. The value of this swirl ratio $\beta = 0.382$ at

$r^* = 0.9$ in the isothermal case is in good agreement with the one provided by the correlation $\beta = 0.49 - 0.57h/b = 0.409$ given by Daily et *al.* [6] for fully turbulent flows. So, for this set of parameters, the mean flow corresponds to the regime IV of Daily and Nece [7]: turbulent flow with separated boundary layers (see also Fig.5).

The influence of Ra remains weak as the maximum value of the convective Rossby number reached for $Ra = 10^8$ is equal to 0.293. It confirms the previous results of Serre et *al.* [22] at lower Reynolds ($Re = 110000$) and Rayleigh ($Ra = 2 \times 10^6$) numbers. For example, the value of the swirl ratio $\beta = 0.382$ at $r^* = 0.9$ obtained in the isothermal case remains the same within less than 1% at this radius even for the largest value of Ra. The maximum difference on β reach 1.5% at $r^* = 0.5$. The influence of Ra is more noticeable by looking at the profiles of the mean radial and axial velocity components. Even though there are no significant changes on the maximum of V_r^* in the Ekman layer, there is a strong modification of the inflow in the Bödewadt layer. At $r^* = 0.9$, there is a decrease of 14% on the minimum of V_r^* between $Ra = 10^6$ and $Ra = 10^8$. This decrease reach 26% at mid-radius. For all radial locations, the axial flow reflected in the V_z^*-values remains very weak compared to the main tangential flow, whatever the value of Ra. The reason is that for these parameters, the convective Rossby number is small, whereas the Taylor number is large. Thus, the bulk flow is in the thermal wind balance and so vertical motion is independent of the vertical coordinate. As no-slip boundary conditions are imposed on the boundaries, the vertical motion is very weak.

Turbulence is mainly confined in the boundary layers where the peak values of the normal components of the Reynolds stress tensor are obtained (Fig.5). On the other side, the central core remains almost laminar. The turbulence intensities are rather the same in both boundary layers with values of R_{rr}^* and $R_{\theta\theta}^*$ much larger than the ones of R_{zz}^*. Note that the values of the cross-components, not shown here, are rather weak in the whole cavity. The influence of the Rayleigh number Ra on the turbulent field is quite weak for Ra up to 10^6. Turbulence intensities slightly increase with Ra in the boundary layers for $0 \leq Ra \leq 10^6$. The maximum values of the normal stresses increase indeed at least of 7% compared to the isothermal case. There are two exceptions: the maxima of R_{rr}^* and R_{zz}^* in the Bödewadt layer at $r^* = 0.9$, where peripheral effects may appear, are almost constant whatever the Rayleigh number. For the highest value of the Rayleigh number $Ra = 10^8$ considered here, there is a strong increase of R_{zz}^* especially for $0.3 \leq r^* \leq 0.7$. For these radial locations,

some plumes similar to the ones shown in Figures 3,8 appear and enhance turbulence in the axial direction. For $r^* = 0.9$ where they are not obtained, the component R^*_{zz} remains rather the same whatever the Rayleigh number.

B. Temperature field

Figure 6 exhibits the temperature profiles along the axial direction for four Rayleigh numbers at four radial locations. Whatever the radial location r^*, the temperature is almost constant and equal to zero in the core of the flow whatever Ra. Nevertheless, two cases have to be distinguished: $Ra = 0$ for which temperature can be considered as a passive scalar and $Ra \neq 0$, for which temperature has an influence on the hydrodynamic field. Thus, for $Ra = 0$, the thermal boundary layers coincide with the Ekman and Bödewadt layers from the hydrodynamic field. The structure of the thermal field is so a Batchelor-like structure. For $Ra \neq 0$, the thermal boundary layers are thicker than the velocity boundary layers as the Prandtl number Pr, which is the ratio of the velocity boundary layer thicknesses to the thermal boundary layer thicknesses is lower than unity ($Pr = 0.7$).

From the axial profiles of T^* (Fig.6), we can deduce the values of the thermal boundary layer thicknesses, denoted δ_{R_T} for the rotor side and δ_{S_T} for the stator one. δ_{R_T} (respectively δ_{S_T}) is the height at which the mean temperature reaches -0.01 (resp. 0.01). δ_{S_T} is found to be larger than δ_{R_T}, which confirms the preponderant influence of the heated disk on thermal convection. For a given Rayleigh number, $Ra = 10^3$ for example, both thermal boundary layers strongly vary with the radial location. δ_{R_T}/H increases from 0.08 at $r^* = 0.3$ to 0.15 at $r^* = 0.9$. In the same time, δ_{S_T}/H decreases from 0.17 to 0.06.

At a given radius, when Ra is increased, it means when the temperature difference is increased, the axial extension of the core decreases as the thermal boundary layers thicken. At $r^* = 0.3$, δ_{R_T}/H (resp. δ_{S_T}/H) increases from 0.08 (resp. 0.17) for $Ra = 10^3$ to 0.19 (resp. 0.53) for $Ra = 10^8$. In the similarity area $0.3 \leq r^* \leq 0.7$, the temperature of the fluid at the edge of the stator boundary layer is increased with Ra due to the main influence of the heated disk. On the other hand, at $r^* = 0.9$ where the cold fluid coming from the shroud is mixed with the hot fluid flowing along the stator, a small decrease appears in the axial profiles of temperature.

The results of figure 6 are confirmed by the radial distributions of T^* shown in figure 7 for

both boundary layers and the same values of Ra. T^* slightly increases with the radius along the rotor apart from some peripheral effects. On the stator side, T^* is almost constant close to the axis and strongly decreases towards the periphery. The radial extent of the region of constant temperature decreases rapidly with the Rayleigh number. The magnitude of T^* is almost constant whatever $Ra \neq 0$ and then diminishes for $Ra = 0$. We recall that, in that case, the temperature can be considered as a passive scalar. Note that T^* tends to 0 at the corner between the insulating hub ($r^* = 0$) and the rotor, where an intense mixing is obtained and tends to 1 at the corner between the insulating shroud ($r^* = 1$) and the rotor. In the same way, T^* tends to the stator temperature at the junction hub-stator ($r^* = 0$) and to 0 at the junction stator-shroud ($r^* = 1$).

C. Heat fluxes along the disks

Figure 8 shows the iso-values of the turbulent heat fluxes as well as the ones of the turbulent temperature fluctuations in a (r, z) plane for $Ra = 10^7$. All these quantities are close to zero around mid-plane and increase in magnitude towards the disks with a magnitude of order 10^{-3}, which confirms the experimental results of Djaoui and Debuchy [8] for the closed cavity. The highest values of these correlations are observed along the hub and along the heated stationary disk. $\overline{v_z't'}$ is found to be different from zero along the disks and in particular along the stator, which is a characteristic of three-dimensional turbulent boundary layers [11]. Areas with positive values of $\overline{v_r't'}$ and especially of $\overline{v_z't'}$ and $\overline{t'^2}$ along the stator correspond to the thermal plumes already observed from the isotherms in Figure 3a. The axial extension of these plumes increases towards the periphery of the cavity. There is a close relationship between the axial heat flux and the temperature fluctuations, contrary to the single disk case, where Elkins and Eaton [11] obtained a stronger relationship between $\overline{v_r't'}$ and $\overline{t'^2}$. This difference may be attributed to the radial confinement in the present study, which induces strong axial flows along the inner and outer cylinders. It is noteworthy that $\overline{v_\theta't'}$ is almost equal to zero in the whole cavity, which confirms the vertical structure of the plumes.

One interesting parameter for numerical modeling is the turbulent Prandtl number Pr_t, defined here as the ratio of the eddy diffusivity for momentum to the eddy diffusivity for heat:

$$Pr_t = \frac{-\overline{v'_\theta v'_z}\frac{\partial \overline{T}}{\partial z}}{\overline{v'_z t'}\frac{\partial \overline{V_\theta}}{\partial z}} \tag{14}$$

Even though is not a rigorous definition of Pr_t for a three-dimensional turbulent boundary layer, where Pr_t should be a second-order tensor, this definition is the one used Elkins and Eaton [11] and appears simpler to enable direct comparisons with the results of these authors. Moreover, this definition deals with the vertical direction along which the thermal plumes are aligned. Typical values of the turbulent Prandtl number are around unity. Pr_t is strictly equal to 1 in accordance with the Reynolds analogy and equal to 0.9 in classical RANS models.

The distributions of the turbulent Prandtl number in the disk boundary layers are shown in Figure 9 for $Ra = 10^7$ and four radial locations. z/δ_R and z/δ_S represent the distances from the rotor and the stator respectively, with δ_R and δ_S the boundary layer thicknesses along the rotor and the stator deduced from the velocity profiles (Fig.4). The same evolution is obtained along both disks. The influence of the radial location remains weak apart at $r^* = 0.9$, where Pr_t is lower close to the disks than at the other radii. The averaged value of Pr_t for $0.3 \leq r^* \leq 0.9$ decreases from 1.4 very close to the disk to about 0.3 at the edge of the boundary layer. The assumption of $Pr_t \simeq 0.9$ is consistent for z/δ_R or z/δ_S up to 0.25 but this level is too high over most of the outer layers. These results are consistent with the measurements of Elkins and Eaton [11] for the turbulent flow over a rotating disk. They obtained $Pr_t \simeq 1.2$ (uncertainty of about 17%) at the disk surface and Pr_t decreases monotically to 0.5 in the outer layer. These values are slightly lower than the ones obtained by Wroblewski [25] in a two-dimensional turbulent boundary layer, where Pr_t decreases to 0.8 at the edge of the boundary layer. The present results and the ones of Elkins and Eaton [11] indicate so that the diffusivity for momentum is reduced more than the diffusivity for heat. Nevertheless, according to Kays [15], the concepts of eddy viscosity and eddy diffusivity are not valid in three-dimensional turbulence and consequently, the turbulent Prandtl number has no meaning. Since the Ekman and Bödewadt boundary layers are three-dimensional turbulent boundary layers, the conclusions on the distributions of Pr_t must be considered tentative.

The effect of the Rayleigh number Ra on the local Nusselt number Nu along the two disks is investigated in figure 10 for given Reynolds $Re = 10^6$ and Prandtl $Pr = 0.7$ numbers.

Apart from some peripheral effects for r^* very close to 0 and 1, Nu is an increasing function of the radial location. It can be explained for the rotor side by looking at the radial distribution of the relative velocity $V^*_{rel} = [(1-V^*_\theta)^2+V^{*2}_r]^{1/2}$ (Fig.11). In the region $0.2 \leq r^* \leq 0.95$, when moving towards the periphery of the cavity, higher velocities are obtained which enhance the heat transfer coefficient reflected in the Nu values. Moreover the relative velocity is almost constant whatever the Rayleigh number, which may explain the weak influence of Ra on the local Nusselt number distribution. A second explanation has been provided by Dorfman [10], which showed that the local Nusselt number varies proportionally to the square root of the local Reynolds number $Re_r = \Omega r^2/\nu$ and so varies linearly with the radial location. Along the rotor side, this linear dependence is obtained (see Fig.10) at $Ra = 0$ for $0.145 \leq r^* \leq 0.68$: $Nu = 470r^* + 160$. The radial extension of this zone decreases when the Rayleigh number increases. On the stator, the linear dependence is obtained at $Ra = 0$ for a much larger radial domain $0.02 \leq r^* \leq 0.85$: $Nu = 440r^* + 140$. Two cases have to be distinguished: $Ra = 0$ (T^* is a passive scalar) and $Ra \neq 0$. As soon as $Ra \neq 0$, there is a strong decrease of Nu in the main part of the cavity. For $10^3 \leq Ra \leq 10^8$, there is no significant effect of the Rayleigh number on the radial distribution of Nu apart from at the junction between the rotor and the hub and at the junction between the stator and the shroud where an intense turbulent mixing between cold and hot fluids appears (see also Fig.3a). In these zones, Nu increases with the Rayleigh number in agreement with previous results described in Owen and Rogers [17].

In the present case, our numerical results can be correlated by:

$$Nu \propto Re_r^{0.7} \tag{15}$$

Thus, the local Nusselt number depends to the local Reynolds number to the power $\gamma = 0.7$. This exponent is close to the one $\gamma = 0.746$ given by Pellé and Harmand [18] (Eq.3) for turbulent flows in an open rotor-stator cavity. It confirms that the Nusselt number is generally lower in an enclosed domain than in an unbounded one [12]. The value of γ falls between the classical values given by Owen and Rogers [17] in the single disk case for the laminar regime $\gamma = 0.5$ and for the turbulent regime $\gamma = 0.8$, confirming the turbulent nature of the flow in our case. The present calculations are also in good agreement with the empirical correlation of Yu et *al.* [26] in the same configuration (turbulent flow enclosed between a lower heated stationary disk and an upper cooled rotating disk for $Re > 1.5 \times 10^5$)

with the terms corresponding to the superimposed mass flow rate set to zero.

Figure 12 presents the dependence of the averaged Nusselt number Nu_{av} on the Rayleigh number for both disks. The inner and outer cylinders being insulated, the overall energy balance implies that the averaged Nusselt numbers are the same along both disks. Here, Nu_{av} is the average value of Nu over the range $0.05 \leq r^* \leq 0.95$. Thus, one removes the strong peripheral effects, which appear in the values of the local Nusselt number close to the inner and outer cylinders (Fig.10). That is why Nu_{av} appears slightly higher on the rotating disk. Nevertheless, for both disks, the evolution remains the same: Nu_{av} decreases with Ra up to $Ra = 10^5$ and then increases. Thus, the results for the averaged Nusselt number on the rotor and stator can respectively be scaled by:

$$Nu_{av} = 3.7(ln(Ra))^2 - 38ln(Ra) + 420 \tag{16}$$

$$Nu_{av} = 4.9(ln(Ra))^2 - 47ln(Ra) + 400 \tag{17}$$

The present value obtained for $Ra = 0$ along the stator is close to the one $Nu_{av} = 496.6$ provided by the correlation given by Poncet and Schiestel [19] (Eq.6) also for $Ra = 0$ along the stator. The weak difference may be attributed to the confinement effects and to the insulating conditions imposed on the cylinders in the present case.

From these results, we can deduce the values of the Bolgiano length L_B, which is the typical length characterizing the forcing mechanism in a convective system defined as:

$$L_B = (\frac{\varepsilon^5}{(g\alpha)^6 N^3})^{1/4} \tag{18}$$

where ε is the turbulence kinetic energy dissipation rate, N the temperature variance dissipation rate and α the thermal expansion coefficient of the fluid. Even though this length scale is a local quantity, Chillá et *al.* [3] proposed an estimate of the averaged value valid for $Nu >> 1$ (which is the case here):

$$< L_B > /H = (\frac{Nu_{av}^2}{RaPr})^{1/4} \tag{19}$$

The turbulent dynamics below the Bolgiano length L_B is unaffected by buoyancy effects, while above it, it may be strongly influenced by the temperature fluctuations, because of their active feedback on the velocity field (see Eq.7). From Equation 19, we can estimate

the mean value of $< L_B > /H$ in the two boundary layers as a function of the Rayleigh number (Fig.13a).

As the mean values of the Nusselt number Nu_{av} are rather the same in the two boundary layers, the evolution with the Rayleigh number of $< L_B > /H$ is rather the same too along both disks. $< L_B > /H$ is almost equal to 3.5 for $Ra = 10^3$. It means that temperature fluctuations can not have any influence in the system. The same remark can be done at $Ra = 10^5$, where $< L_B >$ is still larger than the interdisk spacing H. To conclude if the temperature fluctuations may have an influence in the system, it is required to compare $< L_B >$ with the boundary layer thicknesses. The distributions of $< L_B > /H$ in both boundary layers have been first averaged using the laws (16) to get only one trend curve as these distributions are quite similar. This curve is plotted on Figure 13b. It is compared to the extrema values of δ_{R_T} and δ_{S_T} obtained in the similarity area $0.3 \leq r^* \leq 0.9$. From Figure 13b, it can be seen that δ_{R_T} is lower than $< L_B >$ whatever the radial location for $Ra \leq 10^7$ and gets larger for $Ra = 10^8$ for the whole radial extent. For this value of Ra, temperature fluctuations may have a large influence on the dynamics only at the largest scales of the system. In the same time, $\delta_{S_T} \geq < L_B >$ for $Ra \geq 10^6$ whatever r^*. It confirms that heat transfers are enhanced along the stator and that the thermal plumes appear to be larger on this disk than on the rotor as shown in Figure 3a.

V. CONCLUSION

A numerical investigation of turbulent non-isothermal flows within a shrouded rotor-stator cavity has been performed. The highly accurate computation of turbulent rotating flows within finite cavity is of interest for both engineering applications and fundamental research.

The results of a Large Eddy Simulation using a 3D spectral code stabilized with a Spectral Vanishing Viscosity model already favorably compared to velocity measurements in the isothermal case [23] have been here extended to the non-isothermal case. For $Re = 10^6$ and $G = 5$, the base flow is turbulent and exhibits a Batchelor-like structure with two boundary layers separated by an inviscid rotating core, belonging to the regime IV of Daily and Nece [7]. Turbulence is mainly confined in the boundary layers, whereas the core remains laminar.

Buoyancy effects have been investigated under the Boussinesq approximation for Rayleigh

numbers up to $Ra = 10^8$ and a given Prandtl number $Pr = 0.7$. Some instantaneous views of the velocity and temperature fields have been provided and reveal that the temperature field is strongly affected by the hydrodynamic structures even at large Ra values. The averaged results show small effects of density variation on the mean and turbulent hydrodynamic fields. The main features of non-isothermal turbulent rotor-stator flows have been caught by the LES and compared to previous results. The turbulent Prandtl number decreases from 1.4 at the walls to 0.3 at the edge of the boundary layers. The local Nusselt number is found to be proportional to the local Reynolds number to the power $\gamma = 0.7$. This exponent is close to the one $\gamma = 0.746$ given by Pellé and Harmand [18] for turbulent flows in an open rotor-stator cavity, which confirms that the Nusselt number is generally lower in an enclosed domain than in an unbounded one. Correlations for the averaged Nusselt number on both disks as a function of the Rayleigh number are also provided. The evolution of the averaged Bolgiano length scale $< L_B >$ with the Rayleigh number indicates that temperature fluctuations may have a large influence on the dynamics only at the largest scales of the system for $Ra \geq 10^7$, since $< L_B >$ remains lower than the thermal boundary layer thicknesses.

Further computations are now required to extend these results for industrial flow regimes ($Re = 10^8, Ra = 10^{12}$) and to investigate the influence of rotation on turbulent Rayleigh-Bénard convection for Ro_c close to 1. It implies that for $Re = 10^6$, the Rayleigh number should be equal to $Ra = 1.17 \times 10^9$.

Acknowledgments

The authors acknowledge the IDRIS (CNRS, Orsay, France) computing center where the computations have been carried out on the NEC SX-5 supercomputer (program 070242).

---

[1] K. Abe, T. Kondoh and Y. Nagano. A two-equation heat transfer model reflecting second-moment closures for wall and free turbulent flows. *Int. Heat Fluid Flow*, 17:228–237, 1996.

[2] D. Bohn, J. Ren and C. Tuemmers. Investigation of the unstable flow structure in a rotating cavity. *Proc. of the ASME Turbo Expo 2006: Power for Land, Sea and Air*, Barcelona, May 2006.

[3] F. Chillá, S. Ciliberto, C. Innocenti and E. Pampaloni. Boundary layers and scaling properties in turbulent thermal convection. *Nuovo Cimento D*, 15:1229, 1993.

[4] T. Craft, H. Iacovides, B.E. Launder and A. Zacharos. Some swirling-flow challenges for turbulent CFD. *Flow, Turbulence and Combustion*, 80:419–434, 2008.

[5] O. Czarny, H. Iacovides and B.E. Launder. Precessing Vortex Structures in Turbulent Flow within Rotor-Stator Disc Cavities. *Flow, Turbulence and Combustion*, 69:51–61, 2002.

[6] J.W. Daily, W.D. Ernst and V.V. Asbedian. Enclosed rotating disks with superposed through-flow. *Hydrodynamics Laboratory Report n°64, M.I.T, Department of Civil Engineering*, 1964.

[7] J.W. Daily and R.E. Nece. Chamber dimension effects on induced flow and frictional resistance of enclosed rotating disks. *ASME J. Basic Eng.*, 82:217–232, 1960.

[8] M. Djaoui and R. Debuchy. Heat transfer in a rotor-stator system with a radial inflow. *C.R. Acad. Sci. Paris IIb*, 326:309-314, 1998.

[9] M. Djaoui, A. Dyment and R. Debuchy. Heat transfer in a rotor-stator system with a radial inflow. *Eur. J. Mech. B - Fluids*, 20:371-398, 2001.

[10] L.A. Dorfman. Hydrodynamic Resistance and Heat Loss from Rotating Solids. *Oliver & Boyd*, Edinburgh and London, 1963.

[11] C.J. Elkins and J.K. Eaton. Turbulent heat and momentum transport on a rotating disk. *J. Fluid Mech.*, 402:225-253, 2000.

[12] A.V. Getling. Rayleigh-Bénard convection: structure and dynamics. *Advances in Nonlinear Dynamics*, Vol.11, World Scientific, Singapore, 1998.

[13] S. Harmand, B. Watel and B. Desmet. Local convective heat exchanges from a rotor facing a stator. *Int. J. Therm. Sci.*, 39:404-413, 2000.

[14] H. Iacovides and J.W. Chew. The computation of convective heat transfer in rotating cavities. *Int. Heat Fluid Flow*, 14 (2):146-154, 1992.

[15] W.M. Kays. Turbulent Prandtl Number - where are we ? *Transaction of the ASME*, 116:284-295, 1994.

[16] R.P.J. Kunnen, H.J.H. Clercx, B.J. Geurts, L.J.A. Van Bokhoven, R.A.D. Akkermans and R. Verzicco. Numerical and experimental investigation of structure function scaling in turbulent Rayleigh-Bénard convection. *Phys. Rev. E*, 77:016302 (16 pages), 2008.

[17] J. M. Owen and R. H. Rogers. Flow and Heat Transfer in Rotating-Disc Systems - Vol. 1: Rotor-Stator Systems. *Ed. W. D. Morris, John Wiley and Sons Inc.*, New-York, 1989.

[18] J. Pellé and S. Harmand. Heat transfer measurements in an open rotor-stator system air-gap. *Exp. Therm. Fluid Sci.*, 31:165-180, 2007.

[19] S. Poncet and R. Schiestel. Numerical modelling of heat transfer and fluid flow in rotor-stator cavities with throughflow. *Int. J. Heat Mass Transfer*, 50:1528–1544, 2007.

[20] R.P. Roy, G. Xu and J. Feng. A study of convective heat transfer in a model rotor-stator disk cavity. *ASME J. Turbomach.*, 123:621–632, 2001.

[21] R. Schiestel, L. Elena and T. Rezoug. Numerical modeling of turbulent flow and heat transfer in rotating cavities. *Numer. Heat Trnasfer A*, 24:45–65, 1993.

[22] E. Serre, P. Bontoux and B. Launder. Transitional-turbulent flow with heat transfer in a closed rotor-stator cavity. *J. of Turbulence*, 5, 008, 2004.

[23] E. Séverac, S. Poncet, E. Serre and M.P. Chauve. Large Eddy Simulation and Measurements of Turbulent Enclosed Rotor-Stator Flows. *Phys. Fluids*, 19:085113, 2007.

[24] E. Séverac and E. Serre. A spectral vanishing viscosity LES model for the simulation of turbulent flows within rotating cavities. *J. Comp. Phys.*, 226(6):1234-1255, 2007.

[25] D.E. Wroblewski. An experimental investigation of turbulent heat transport in a boundary layer with an embedded streamwise vortex. *PhD thesis, University of California*, Berkeley, 1990.

[26] J.P. Yu, E.M. Sparrow and E.R.G. Eckert. Experiments on a shrouded, parallel disk system with rotation and coolant throughflow. *Int. J. Heat Mass Transfer*, 16:311–328, 1973.

- Fig.1: Scheme of the enclosed rotor-stator cavity with relevant notation. Example of the mesh grid within the stator boundary layer (only one-fourth of the points are shown).

- Fig.2: Iso-values at $Ra = 10^7$ of the instantaneous normal temperature gradient $\partial T^*/\partial z^*$ at the (a) rotor surface and at the (b) stator surface and of the instantaneous tangential velocity V_θ normalized by the maximum disk speed Ωb in (c) the rotor boundary layer layer ($z^* = 0.97$) and in (d) the stator boundary layer ($z^* = 0.03$).

- Fig.3: Iso-values of (a) the instantaneous temperature T^* and (b) the instantaneous axial velocity V_z normalized by Ωb at $Ra = 10^7$ in a (r, z) plane.

- Fig.4: Axial profiles of the three mean velocity components at four radial locations in the range $0.3 \leq r^* \leq 0.9$ and for four values of the Rayleigh number: (solid lines) $Ra = 0$, (dashed lines) $Ra = 10^3$, (dash-dot lines) $Ra = 10^6$, (dotted lines) $Ra = 10^8$. Comparison with the (points) isothermal case.

- Fig.5: Axial profiles of the three normal Reynolds stress components at four radial locations in the range $0.3 \leq r^* \leq 0.9$ and for four values of the Rayleigh number: (solid lines) $Ra = 0$, (dashed lines) $Ra = 10^3$, (dash-dot lines) $Ra = 10^6$, (dotted lines) $Ra = 10^8$. Comparison with the (points) isothermal case.

- Fig.6: Axial profiles of the mean temperature at four radial locations and for four values of the Rayleigh number: (solid lines) $Ra = 0$, (dashed lines) $Ra = 10^3$, (dash-dot lines) $Ra = 10^6$, (dotted lines) $Ra = 10^8$.

- Fig.7: Radial distributions of the mean temperature T^* along the rotor at $z^* = 0.99$ and along the stator at $z^* = 0.01$ for four values of the Rayleigh number.

- Fig.8: Iso-values of the turbulent heat fluxes (a) $\overline{v_r' t'}$, (b) $\overline{v_\theta' t'}$ and (c) $\overline{v_z' t'}$ normalized by $\Omega b \Delta T$ and of (d) the turbulent temperature fluctuations $\overline{t'^2}/(\Delta T)^2$ at $Ra = 10^7$ in a (r, z) plane.

- Fig.9: Turbulent Prandtl number in the rotor and stator boundary layers for $Ra = 10^7$ and four radial locations.

- Fig.10: Radial distributions of the local Nusselt number Nu along the rotor and the stator for four values of the Rayleigh number Ra.

- Fig.11: Radial distribution of the relative velocity V^*_{rel} along the rotor ($z^* = 0.99$) for four values of the Rayleigh number.

- Fig.12: Influence of the Rayleigh number Ra on the averaged Nusselt number Nu_{av} on both disks.

- Fig.13: (a) Influence of the Rayleigh number Ra on the mean Bolgiano scale $< L_B >$ $/H$ for both boundary layers; (b) Comparison with the thermal boundary layer thicknesses.

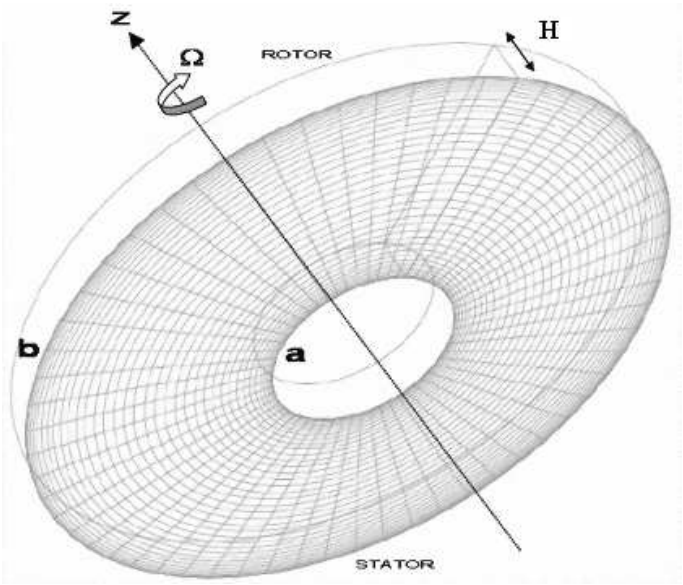

Figure 1: Poncet & Serre, submitted to Int. J. Heat Fluid Flow.

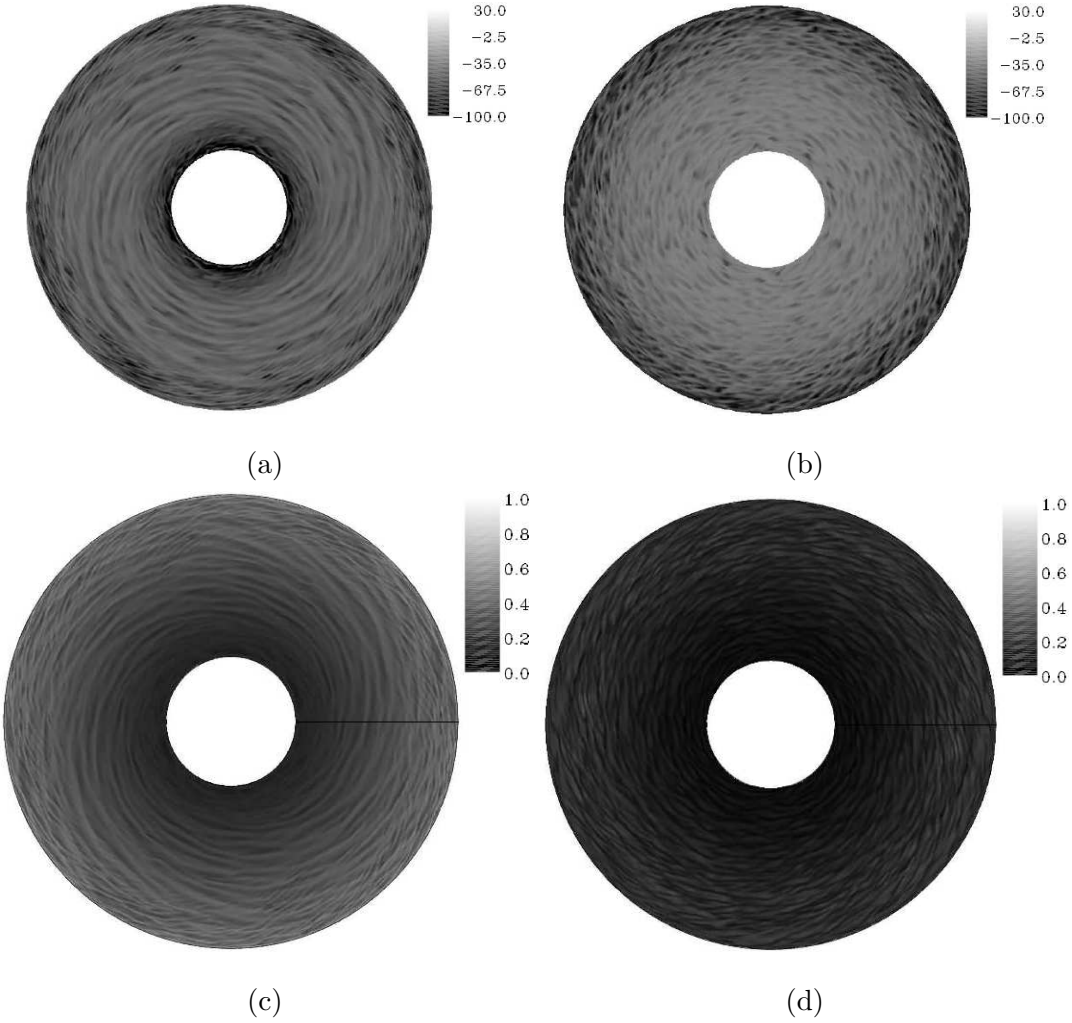

Figure 2: Poncet & Serre, submitted to Int. J. Heat Fluid Flow.

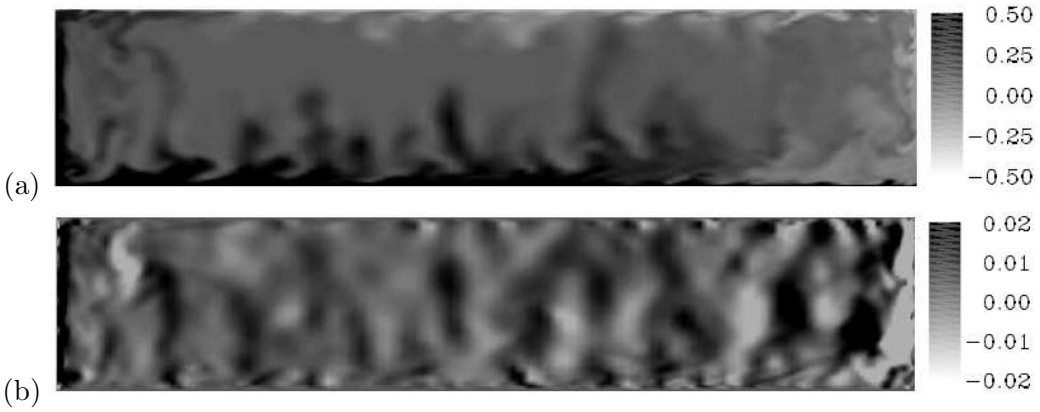

Figure 3: Poncet & Serre, submitted to Int. J. Heat Fluid Flow.

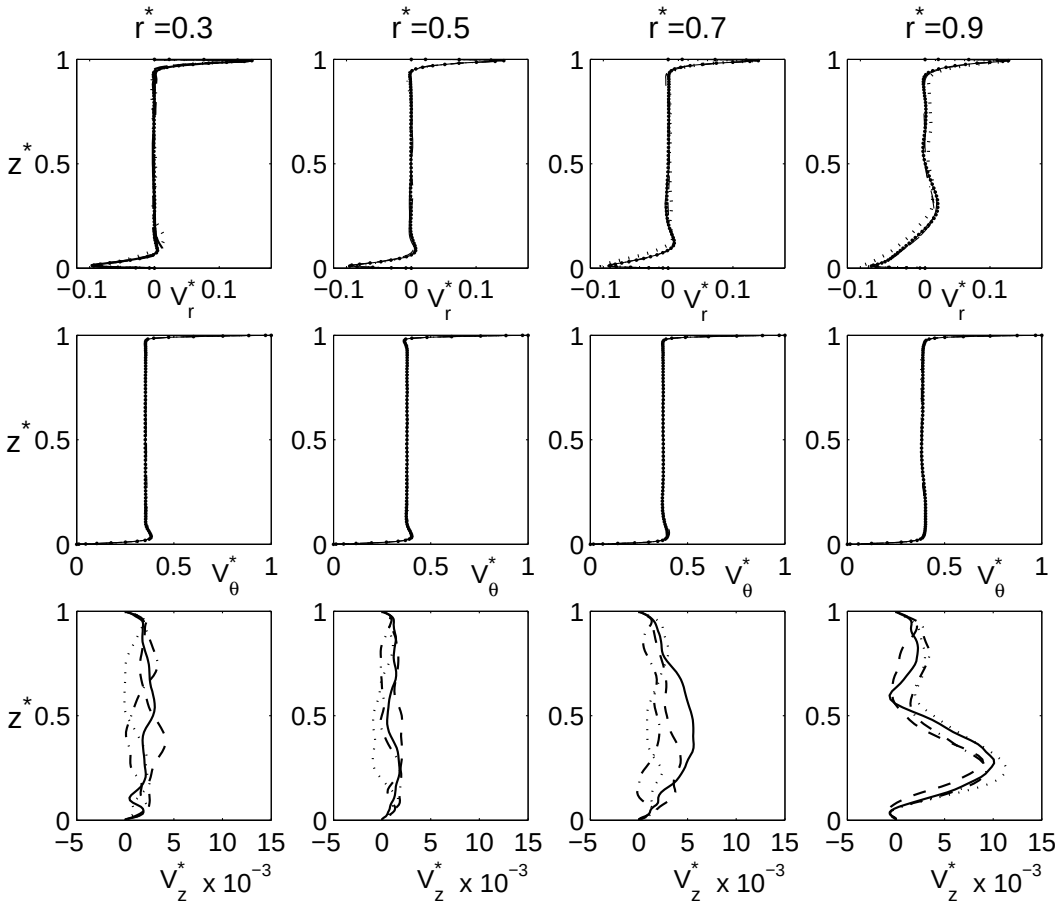

Figure 4: Poncet & Serre, submitted to Int. J. Heat Fluid Flow.

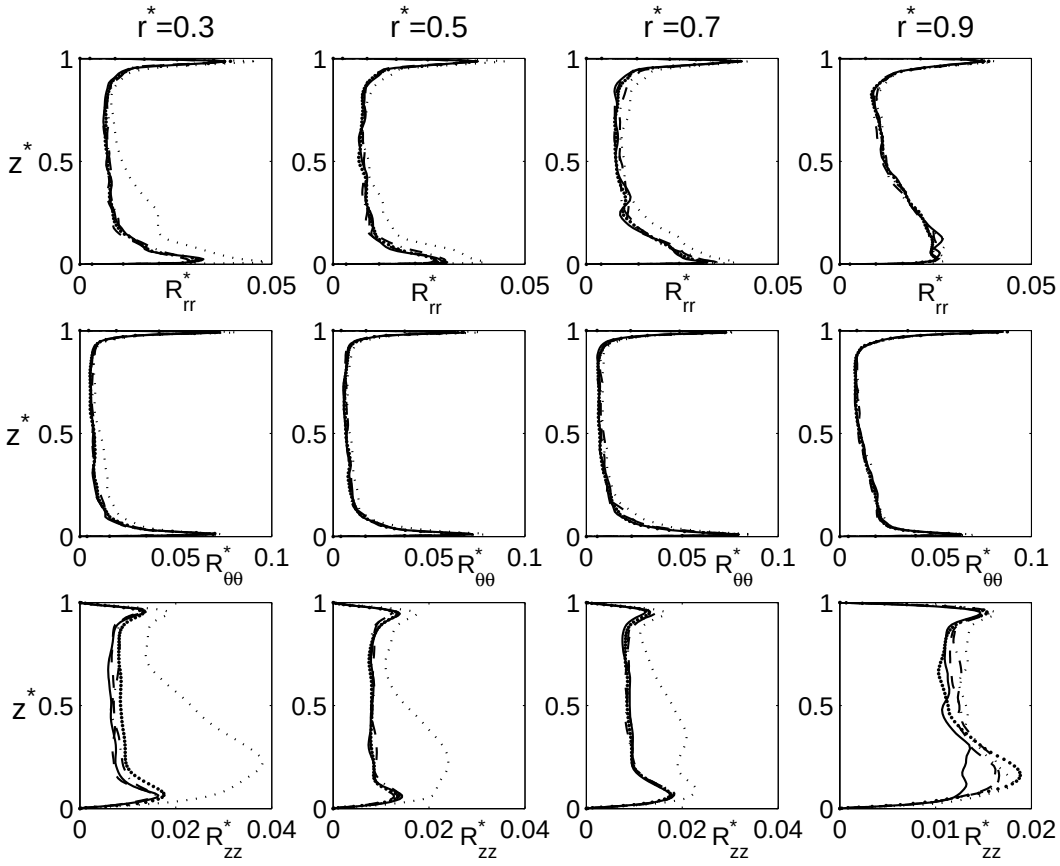

Figure 5: Poncet & Serre, submitted to Int. J. Heat Fluid Flow.

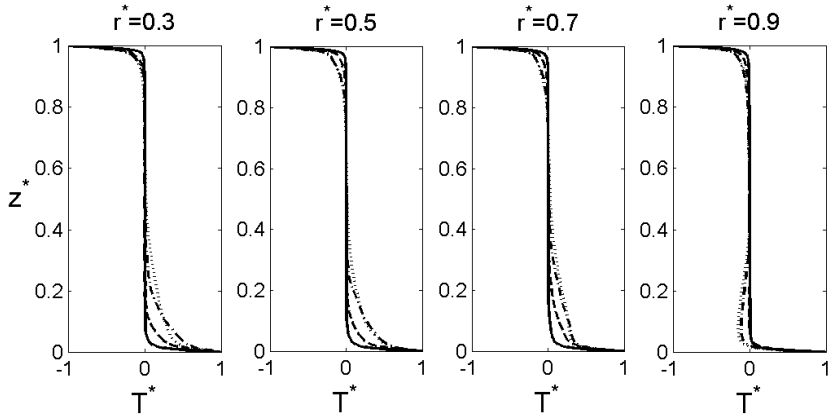

Figure 6: Poncet & Serre, submitted to Int. J. Heat Fluid Flow.

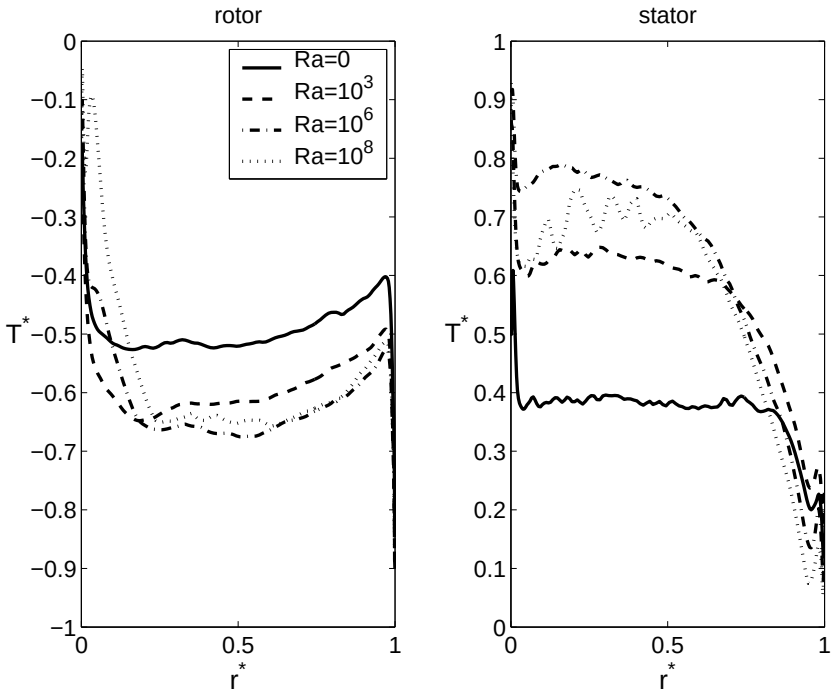

Figure 7: Poncet & Serre, submitted to Int. J. Heat Fluid Flow.

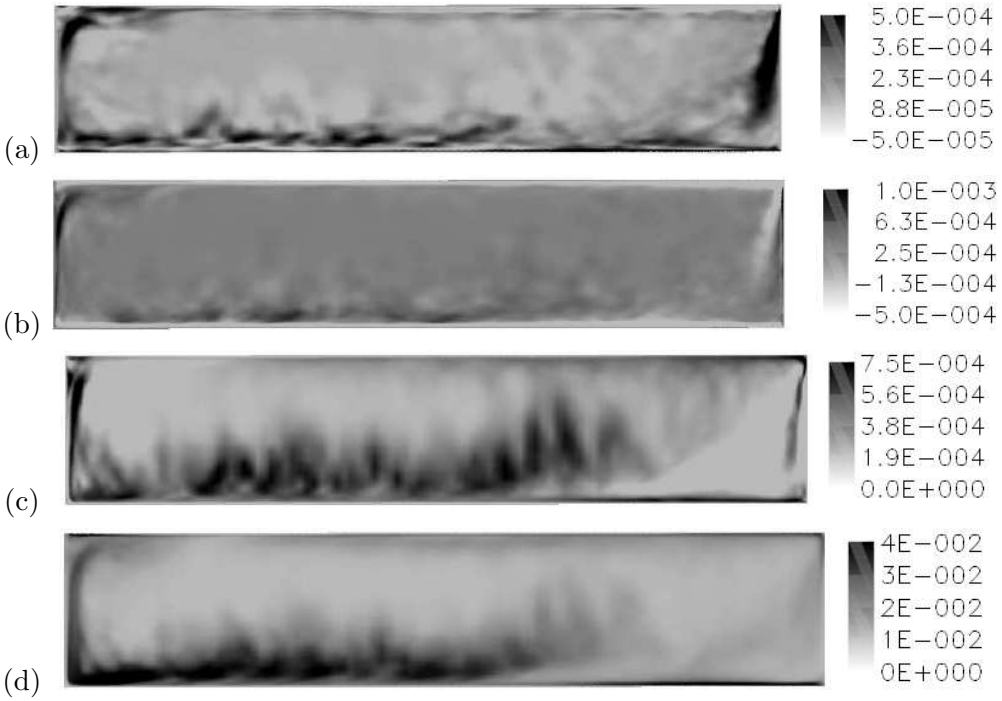

Figure 8: Poncet & Serre, submitted to Int. J. Heat Fluid Flow.

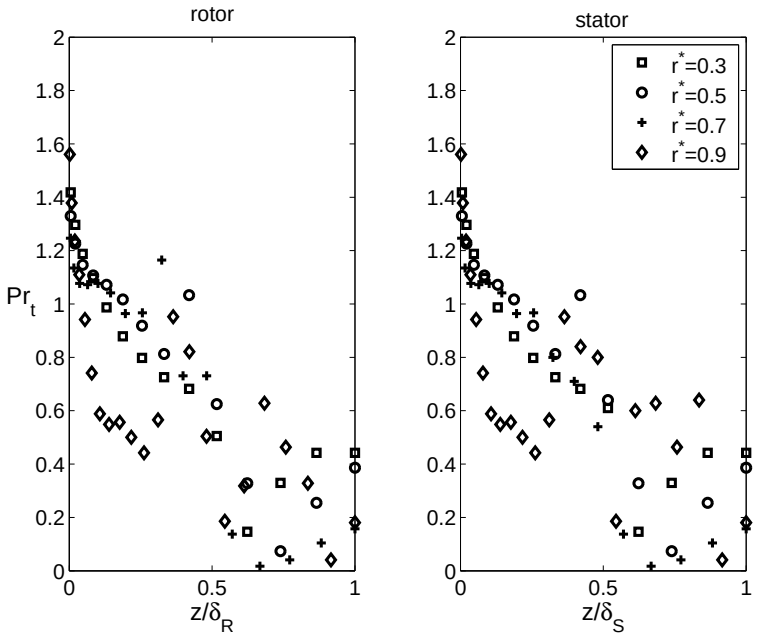

Figure 9: Poncet & Serre, submitted to Int. J. Heat Fluid Flow.

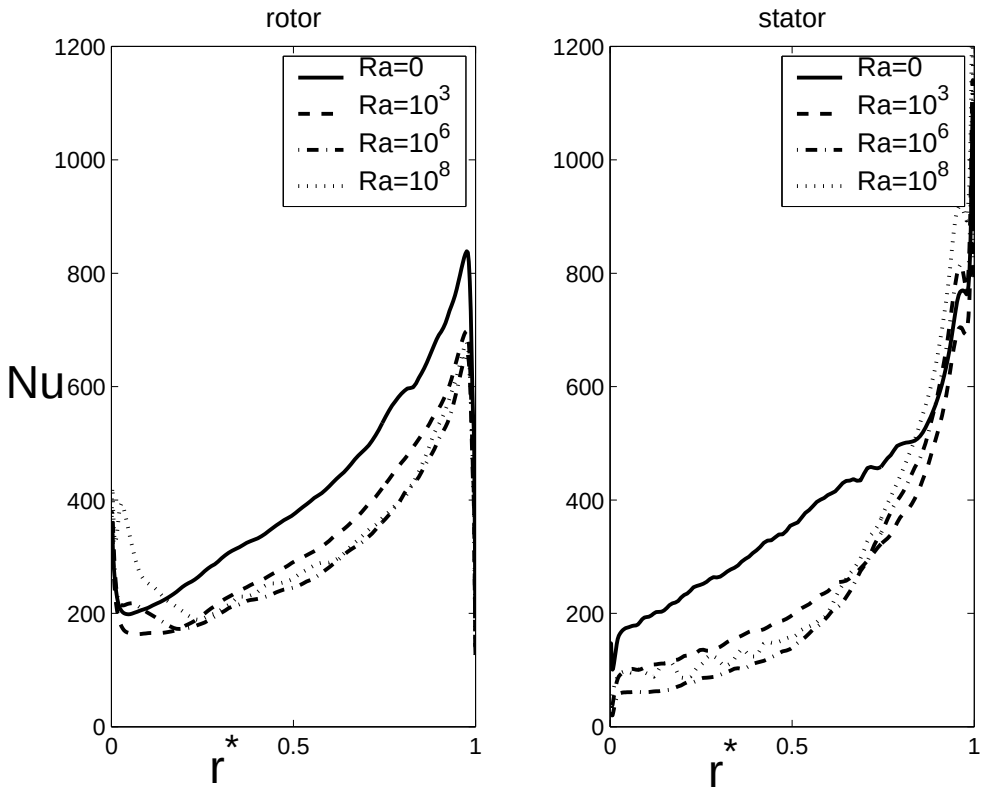

Figure 10: Poncet & Serre, submitted to Int. J. Heat Fluid Flow.

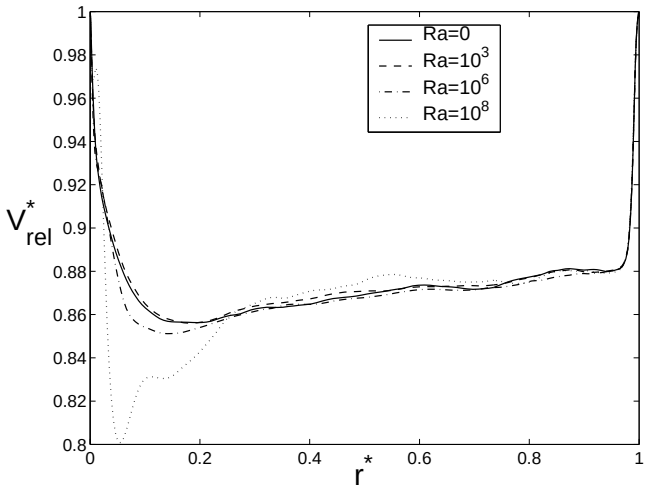

Figure 11: Poncet & Serre, submitted to Int. J. Heat Fluid Flow.

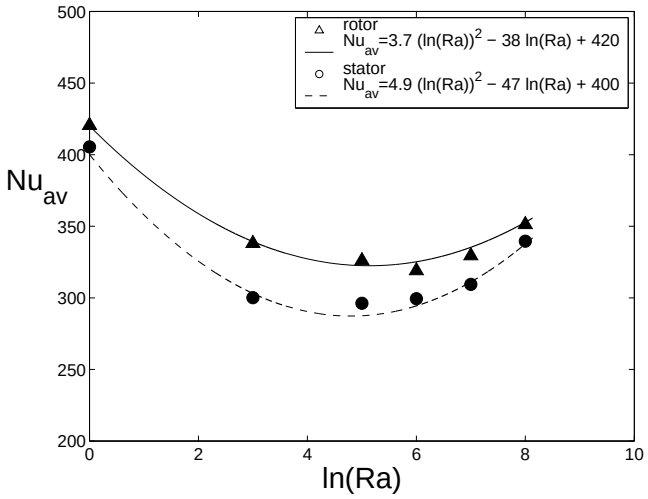

Figure 12: Poncet & Serre, submitted to Int. J. Heat Fluid Flow.

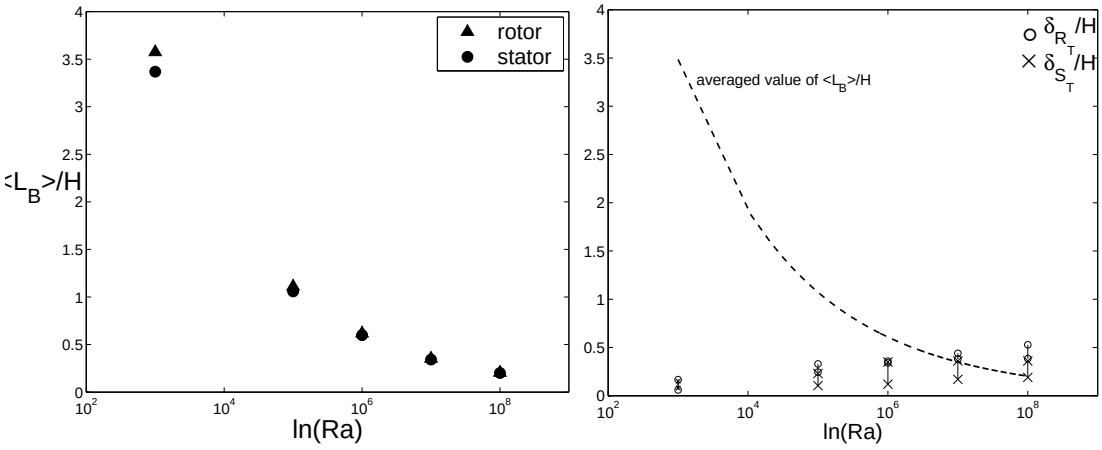

(a) (b)

Figure 13: Poncet & Serre, submitted to Int. J. Heat Fluid Flow.

a	radius of the hub, m
b	outer radius of the rotating disk, m
H	interdisk spacing, m
L_B	Bolgiano length scale, m
r, θ, z	cylindrical coordinates, m
R_{ij}	Reynolds stress tensor with $i, j = (r, \theta, z)$, m^2/s^2
T	mean temperature of the fluid, K
$t^{'}$	temperature fluctuation, K
T_r	temperature of reference
V_r, V_θ, V_z	radial, tangential and axial velocity components, m/s
$v_r^{'}$, $v_\theta^{'}$, $v_z^{'}$	fluctuations of the radial, tangential and axial velocity components, m/s
β	swirl ratio
δ_R, δ_S	the hydrodynamic boundary layer thicknesses along the rotor and the stator respectively, m
δ_{R_T}, δ_{S_T}	the thermal boundary layer thicknesses along the rotor and the stator respectively, m
κ	thermal diffusivity of the fluid, m^2/s
λ	thermal conductivity of the fluid, $W/m.K$
ν	kinematic viscosity of the fluid, m^2/s
Ω	rotation rate of the rotating disk, rad/s
G	aspect ratio of the cavity
Nu	local Nusselt number
Nu_{av}	averaged Nusselt number
Pr	Prandtl number
Pr_t	turbulent Prandtl number
R_m	curvature parameter of the cavity
Ra	Rayleigh number
Re	rotational Reynolds number based on b
Re_r	local Reynolds number based on r
Ro_c	convective Rossby number
Ta	Taylor number
$*$	normalized quantity